

Trajectory Tracking Control of a Four Mecanum Wheeled Mobile Platform: an Extended State Observer-Based Sliding Mode Approach

ISSN 1751-8644
 doi: 0000000000
www.ietdl.org

Zhenyi Yuan¹, Yunfei Yin¹, Siyi Wang¹, Jianxing Liu¹, Ligang Wu^{1*}

¹ School of Astronautics, Harbin Institute of Technology, Harbin 150001, P. R. China

* E-mail: Corresponding author: ligangwu@hit.edu.cn

Abstract: This paper proposes an extended state observer-based sliding mode control (ESO-SMC) strategy for trajectory tracking of a four mecanum wheeled mobile platform (FMWMP) with unknown disturbances and model uncertainties (UDMU) considered. Specially, the extended state observer (ESO) is designed to estimate not only the UDMU, but also the unmeasured velocities of FMWMP. Based on the designed ESO, a sliding mode control (SMC) scheme is utilized to ensure the tracking performance as expected. By using Lyapunov synthesis, it is shown that all the signals of the whole system can be guaranteed to be uniformly ultimately bounded (UUB). To verify the effectiveness of the proposed control strategy, simulations and experiments are carried out with two different kinds of reference trajectories. Furthermore, a comparative work is done to show that the ESO-SMC controller has better control performance than traditional proportional-integral-derivative (PID) controller.

1 Introduction

Recently, with the increasing demands for autonomous maneuverability, wheeled mobile robots have attracted much attention and been broadly applied in many aspects of our society [1–4]. Owing to their enhanced mobility compared with conventional mobile robots, omnidirectional wheeled mobile robots, which are capable to move in confined spaces easily, have been extensively investigated [5–7]. Four mecanum wheeled mobile platform (FMWMP) is one kind of the omnidirectional mobile robot consisting of a rectangular configuration and four mecanum wheels. As shown in Fig. 1, the mecanum wheel is actually a conventional wheel with a series passive rollers attached to its circumference. These rollers normally have a axis of rotation at 45° to the axis of rotation of the wheel. Due to this special structure of mecanum wheels, FMWMP have an extra **degree of freedom (DOF)** with respect to conventional differential-driven wheeled robots, i.e., FMWMP can move in any direction without reorientation.

As the manufacture industry developed rapidly these years, mobile manipulator has become a widespread term for human assistance [8]. To enhance the mobility and flexibility of a mobile manipulator, some researchers intend to design a FMWMP-based manipulator to accomplish tele-operation tasks [9, 10]. It should be stressed that in such situations, trajectory tracking accuracy of FMWMP is the key point to ensure the performance of tele-operation. Thus, a high-precision controller which guarantees the FMWMP tracking the desired trajectory accurately is required. However, in practice, sometimes the FMWMP may enter the region of nonlinear behaviors because of the **unknown disturbances and model uncertainties (UDMU)** [11], leading the FMWMP system to unstable. Therefore, there are still lots of challenges to propose a high-accuracy control strategy for FMWMP.

In order to overcome the control difficulties mentioned above, firstly, the kinematic and dynamic models of a FMWMP have been investigated in several literatures [12–14]. Since FMWMP is a complex nonlinear system, nonlinear control strategies, such as fuzzy control, backstepping control and sliding mode control, perform better than traditional linear control strategy like **proportional-integral-derivative (PID) controller** [15–17]. In [15], a fuzzy wavelet networks approach is proposed to approximate some uncertain

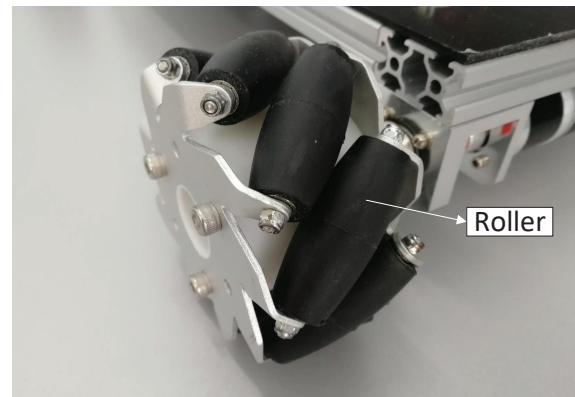


Fig. 1: Structure of a mecanum wheel (a left backward one).

nonlinear terms in controller design; in [16], a backstepping controller combining Neural-Networks approximation is investigated and applied for FMWMP system; in [17], in face of the external disturbances, **sliding mode control (SMC)** is presented to deal with the disturbances. It should be noted that although those nonlinear strategies have been implemented on FMWMP, only the simulation results show the effectiveness and none of them have real experimental validation.

Due to its insensitivity to disturbances, SMC has been gaining more and more attention for suppressing disturbances in complex nonlinear systems [18–24]. It has been extensively employed in the controller design of mobile robots [25–27]. The main disadvantage of SMC is so-called *chattering* phenomenon, caused by discontinuity of the control law, which not only wastes energy but also reduces the trajectory smoothness [28]. Several methods, such as higher order sliding mode control [29] and adaptive sliding mode control [30] have been proposed to suppress chattering. Generally speaking, the UDMU are highly uncertain since the FMWMP usually works exposed to dynamic environment. The SMC scheme may bring serious chattering if the lumped disturbances/uncertainties term goes too large, even lead the FMWMP system to unstable.

One approach to realize UDMU rejection is to design a disturbance-observer (DOB) estimating the UDMU, followed by the SMC controller design to compensate the UDMU [31]. Such DOBs generally include high-gain observer (HGO) [32], sliding mode observer [33] and extended state observer (ESO) [34], etc. It is worth to mention that, unlike traditional observers, ESO is actually one kind of state observer with the lumped disturbances/uncertainties term regarded as a new state of the system. Hence, this kind of observer is conceived to estimate both the plant states and the lumped disturbances/uncertainties term.

Note that another difficulty in controlling of a FMWMP is that there is no sensor available to measure the velocities directly. However, the velocity information is also important in the controller design. Recently, due to its relatively simple structure and good performance, HGO has been developed to estimate unmeasured states and combined with SMC to design output feedback controller in industrial systems [35, 36]. The main disadvantage of HGO is so-called *peaking* phenomenon [37], on which we will give some remarks in Section 5.

In this paper, motivated by the ESO [38, 39] and HGO based SMC [35], we propose an *extended state observer-based sliding mode control (ESO-SMC)* strategy for improving the tracking performance of the FMWMP. Firstly, an ESO is proposed to estimate the lumped disturbances/uncertainties term and unmeasured states. Then based on the estimations, a SMC controller is proposed to ensure the trajectory tracking errors to be *uniformly ultimately bounded (UUB)*. To validate the effectiveness of proposed control method, both simulations and experiments with two kinds of reference trajectories are illustrated, followed by the comparison results between ESO-SMC controller and PID controller. The main contributions of this paper can be summarized as follows:

- (1) A FMWMP model considering the unknown disturbances and model uncertainties is reframed.
- (2) A ESO-SMC scheme is implemented to a FMWMP where the ESO is designed to estimate both the unmeasured velocities and lumped disturbances/uncertainties term.
- (3) Experimental validations on a real FMWMP are taken to show the effectiveness of proposed control strategy. Furthermore, comparative studies with PID controller are carried out.

The rest of this paper is organized as follows: Section 2 presents the mathematical model of FMWMP. In Section 3, an ESO-SMC controller is designed to ensure all the signals of FMWMP system to be UUB. Section 4 and Section 5 show the simulation and experiment results, respectively, followed by the conclusion in Section 6.

Table 1 Nomenclature of this paper

Symbol	Description	Unit
$\dot{\theta}_i (i = 1, \dots, 4)$	Angular velocity of the i_{th} wheel	rad/s
$\tau_i (i = 1, \dots, 4)$	External generalized force generated by the i_{th} DC motor	$N \cdot m$
ϕ_a	Equals to $\phi + \pi/4$	
a	Half of width of the platform	m
b	Half of length of the platform	m
m	Total mass of the platform	kg
R	Radius of mecanum wheel	m
D_θ	Wheel's viscous friction coefficient	
$f_i (i = 1, \dots, 4)$	Static friction of the i_{th} wheel	N
J_ω	Wheel's moment of inertial around the center of the revolution	$N \cdot m$
J_z	Platform's moment of inertial around the center of the revolution	$N \cdot m$
A_j	Constant equals to $\frac{mR^2}{8}$	
B_j	Constant equals to $\frac{J_z R^2}{16(a+b)^2}$	
R_a	Armature resistance of a DC motor	Ω
L_a	Armature inductance of a DC motor	H
K_b	Back electromotive force (EMF) constant of a DC motor	$V \cdot s/rad$
K_m	Torque constant of a DC motor	$N \cdot m/A$

Nomenclature: Throughout this paper, some symbols representing constants or physical quantities are shown in Table 1.

Notations: The superscripts 'T' and '-1' denote the matrix transpose and inverse, respectively. $\|\cdot\|$ represents the Euclidean norm of a vector or the corresponding induced norm of a matrix. $\Delta(\cdot)$ represents the model uncertain term. $(\hat{\cdot})$ represents the estimation value of (\cdot) . $(\cdot)^{(k)}$ represents k-order time derivative of (\cdot) . $\lambda_{max}(\cdot)$ and $\lambda_{min}(\cdot)$ represent the maximum eigenvalue of a matrix and the minimum eigenvalue of a matrix (assume this matrix is a real symmetric matrix), respectively.

2 Mathematical Model of FMWMP

As shown in Fig. 2, $X_q O_q Y_q$ and $X_r O_r Y_r$ are defined as inertial frame and body frame, respectively. The origin of inertial frame represents the geometric center of FMWMP at the initial place while the origin of body frame represents the real-time geometric center of FMWMP. The states of the FMWMP in inertial frame and body frame can be described by $[x_q \ y_q \ \dot{\phi}]$ and $[x_r \ y_r \ \dot{\phi}]$, respectively.

2.1 Kinematics of FMWMP

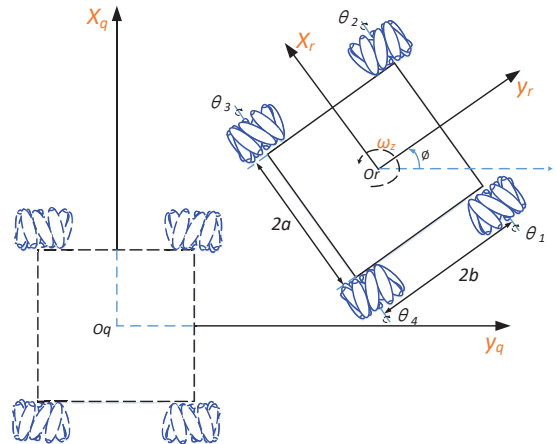


Fig. 2: Structure and frames of a FMWMP.

The kinematic model of the FMWMP is introduced in [13], described by

$$\begin{aligned} R\dot{\theta}_1 &= -\dot{x}_r + \dot{y}_r - \dot{\phi}(a+b), \\ R\dot{\theta}_2 &= \dot{x}_r + \dot{y}_r - \dot{\phi}(a+b), \\ R\dot{\theta}_3 &= -\dot{x}_r + \dot{y}_r + \dot{\phi}(a+b), \\ R\dot{\theta}_4 &= \dot{x}_r + \dot{y}_r + \dot{\phi}(a+b). \end{aligned} \quad (1)$$

Define a matrix

$$J = \begin{bmatrix} -1 & 1 & -(a+b) \\ 1 & 1 & -(a+b) \\ -1 & 1 & (a+b) \\ 1 & 1 & (a+b) \end{bmatrix} \in \mathbb{R}^{4 \times 3}, \quad (2)$$

then (1) can be rewritten as

$$[\dot{\theta}_1 \ \dot{\theta}_2 \ \dot{\theta}_3 \ \dot{\theta}_4]^T = \frac{J}{R} [\dot{x}_r \ \dot{y}_r \ \dot{\phi}]^T. \quad (3)$$

It is noticed that although J is a non-square matrix, there exists a new matrix

$$J^+ = \frac{1}{4} \begin{bmatrix} -1 & 1 & -1 & 1 \\ 1 & 1 & 1 & 1 \\ \frac{1}{a+b} & -\frac{1}{a+b} & -\frac{1}{a+b} & \frac{1}{a+b} \end{bmatrix} \in \mathbb{R}^{3 \times 4}, \quad (4)$$

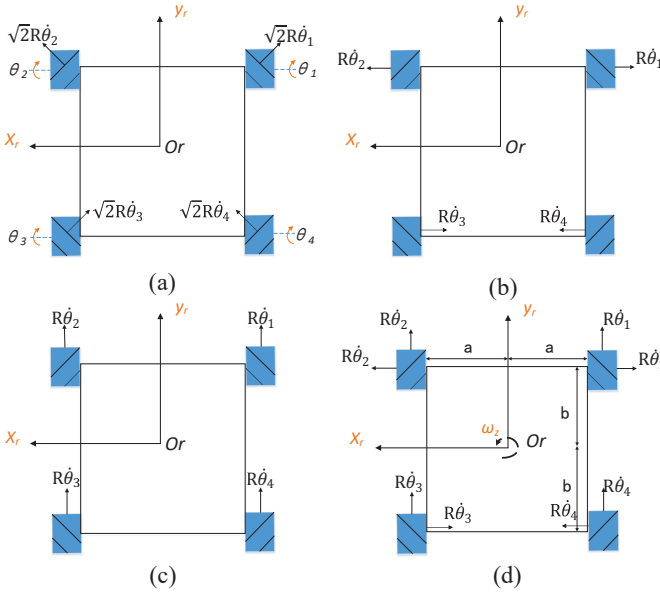


Fig. 3: (a) The velocity of the roller attaches the ground of each mecanum wheel. (b) The velocity along X_r axis produced by the rotations of four mecanum wheels. (c) The velocity along Y_r axis produced by the rotations of four mecanum wheels. (d) The rotation angular velocity along ω_z axis produced by the rotations of four mecanum wheels.

which is the pseudo inverse matrix of J and satisfying $J^+ J = I \in \mathbb{R}^{3 \times 3}$. Note that the structure of matrix J^+ can also be explained by Fig. 3, which illustrates the relationship between the rotations of the mecanum wheels and the movements along three DOFs. In views of (3) and (4), yields

$$[\dot{x}_r \quad \dot{y}_r \quad \dot{\phi}]^T = R J^+ [\dot{\theta}_1 \quad \dot{\theta}_2 \quad \dot{\theta}_3 \quad \dot{\theta}_4]^T. \quad (5)$$

Furthermore, considering the body velocities in the inertial frame one can easily obtain the relationship expressed by

$$[\dot{x}_q \quad \dot{y}_q \quad \dot{\phi}]^T = \mathcal{R}(\phi) [\dot{x}_r \quad \dot{y}_r \quad \dot{\phi}]^T, \quad (6)$$

where $\mathcal{R}(\phi) = \begin{bmatrix} \cos(\phi) & -\sin(\phi) & 0 \\ \sin(\phi) & \cos(\phi) & 0 \\ 0 & 0 & 1 \end{bmatrix}$ represents the rotation matrix of body frame with respect to inertial frame.

2.2 Dynamics of FMWMP

The dynamic model of the FMWMP is derived by using Lagrange's equation, which is proposed in [15], expressed as

$$2(\tau - F) - \frac{\partial D_\theta \sum_{i=1}^4 \dot{\theta}_i^2}{\partial \dot{\theta}} = \frac{\partial}{\partial t} \frac{\partial(m(x_q^2 + y_q^2) + J_z \dot{\phi}^2 + J_\omega \sum_{i=1}^4 \dot{\theta}_i^2)}{\partial \dot{\theta}} - \frac{\partial(m(x_q^2 + y_q^2) + J_z \dot{\phi}^2 + J_\omega \sum_{i=1}^4 \dot{\theta}_i^2)}{\partial \theta}, \quad (7)$$

where

$$\begin{aligned} \tau &= [\tau_1 \quad \tau_2 \quad \tau_3 \quad \tau_4]^T, \\ \theta &= [\theta_1 \quad \theta_2 \quad \theta_3 \quad \theta_4]^T, \\ F &= [f_1 \operatorname{sgn}(\dot{\theta}_1) \quad f_2 \operatorname{sgn}(\dot{\theta}_2) \quad f_3 \operatorname{sgn}(\dot{\theta}_3) \quad f_4 \operatorname{sgn}(\dot{\theta}_4)]^T [40]. \end{aligned}$$

Substituting (5), (6) into (7), one obtains

$$\tau = M \ddot{\theta} + D_\theta \dot{\theta} + F, \quad (8)$$

where

$$M = \begin{bmatrix} A_j + B_j + J_\omega & -B_j \\ -B_j & A_j + B_j + J_\omega \\ B_j & A_j - B_j \\ A_j - B_j & B_j \\ B_j & A_j - B_j \\ A_j + B_j + J_\omega & -B_j \\ -B_j & A_j + B_j + J_\omega \end{bmatrix}.$$

2.3 Unknown Disturbances and Model Uncertainties

Considering the unknown dynamic disturbances and uncertainties, a new dynamic model is obtained as follows

$$\tau + \tau_d = (M + \Delta M) \ddot{\theta} + (D_\theta + \Delta D_\theta) \dot{\theta} + F + \Delta F, \quad (9)$$

where τ_d is the unknown disturbances term.

Then, put the uncertain terms ΔM , ΔD_θ and ΔF on the left side and one can obtain

$$\tau + \tau_d + H_d = M \ddot{\theta} + D_\theta \dot{\theta} + F, \quad (10)$$

where $H_d = -\Delta M \ddot{\theta} - \Delta D_\theta \dot{\theta} - \Delta F$.

Assumption 1. The unknown disturbance term $\tau_d(t)$ satisfies $\|\tau_d^{(j)}\| \leq \mu_1$, $j = 0, 1, 2, \dots, n$, where μ_1 is an unknown positive number.

Assumption 2. The uncertain terms ΔM , ΔD_θ and ΔF are bounded. Moreover, the uncertain term H_d satisfies $\|H_d^{(j)}\| \leq \mu_2$, $j = 0, 1, 2, \dots, n$, where μ_2 is an unknown positive number.

Remark 1. In practical robotic engineering, the speed of revolution and its time derivatives of DC motors have the upper bounds, i.e., $\|\dot{\theta}\| \leq \bar{\theta}_1$, $\|\ddot{\theta}\| \leq \bar{\theta}_2, \dots$, $\|\theta^{(j)}\| \leq \bar{\theta}_j$. As ΔM , ΔD_θ and ΔF are related to $\dot{\theta}$ and $\ddot{\theta}$, it can be concluded that the time derivatives of ΔM , ΔD_θ and ΔF are also bounded. Assume that $\|\Delta M^{(j)}\| \leq \bar{\Delta M}$, $\|\Delta D_\theta^{(j)}\| \leq \bar{\Delta D}_\theta$ and $\|\Delta F^{(j)}\| \leq \bar{\Delta F}$, then it can be known that $\|H_d^{(j)}\| \leq \|\Delta M \ddot{\theta}^{(j)}\| + \|\Delta D_\theta \dot{\theta}^{(j)}\| + \|\Delta F^{(j)}\| \leq \sum_{i=0}^j C_j^i (\bar{\Delta M} \|\bar{\theta}_{(j+2-i)}\| + \bar{\Delta D}_\theta \|\bar{\theta}_{(j+1-i)}\|) + \bar{\Delta F}$ and this relaxes the Assumption 2.

2.4 State-Space Representation

Substituting (5), (6) into (10), yields

$$\begin{bmatrix} \ddot{x}_q \\ \ddot{y}_q \\ \ddot{\phi} \end{bmatrix} = -(\mathcal{J}^+(\phi) \dot{\mathcal{J}}(\phi) + D_\theta \mathcal{J}^+(\phi) M^{-1} \mathcal{J}(\phi)) \begin{bmatrix} \dot{x}_q \\ \dot{y}_q \\ \dot{\phi} \end{bmatrix} + R \mathcal{J}^+(\phi) M^{-1} (\tau + \tau_d + H_d - F), \quad (11)$$

where

$$\begin{aligned}\mathcal{J}^+(\phi) &= \begin{bmatrix} \sqrt{2}\sin(\phi_a) & \sqrt{2}\cos(\phi_a) & \sqrt{2}\cos(\phi_a) \\ -\sqrt{2}\cos(\phi_a) & \sqrt{2}\sin(\phi_a) & \sqrt{2}\sin(\phi_a) \\ -\frac{1}{a+b} & \frac{1}{a+b} & -\frac{1}{a+b} \end{bmatrix}, \\ \mathcal{J}(\phi) &= \begin{bmatrix} \sqrt{2}\sin(\phi_a) & -\sqrt{2}\cos(\phi_a) & -(a+b) \\ \sqrt{2}\cos(\phi_a) & \sqrt{2}\sin(\phi_a) & a+b \\ \sqrt{2}\cos(\phi_a) & \sqrt{2}\sin(\phi_a) & a+b \\ \sqrt{2}\sin(\phi_a) & -\sqrt{2}\cos(\phi_a) & -(a+b) \end{bmatrix}, \\ \dot{\mathcal{J}}(\phi) &= \dot{\phi} \begin{bmatrix} \sqrt{2}\cos(\phi_a) & \sqrt{2}\sin(\phi_a) & 0 \\ -\sqrt{2}\sin(\phi_a) & \sqrt{2}\cos(\phi_a) & 0 \\ -\sqrt{2}\sin(\phi_a) & \sqrt{2}\cos(\phi_a) & 0 \\ \sqrt{2}\cos(\phi_a) & \sqrt{2}\sin(\phi_a) & 0 \end{bmatrix}.\end{aligned}$$

Define $Z_1 = [x_q \ y_q \ \dot{\phi}]^T$, $Z_2 = [\dot{x}_q \ \dot{y}_q \ \dot{\phi}]^T$, $H = R\mathcal{J}^+(\phi)M^{-1}(H_d + \tau_d)$, $f(Z_1, Z_2) = (\mathcal{J}^+(\phi)\dot{\mathcal{J}}(\phi) + D_\theta\mathcal{J}^+(\phi)M^{-1}\mathcal{J}(\phi))[\dot{x}_q \ \dot{y}_q \ \dot{\phi}]^T + R\mathcal{J}^+(\phi)M^{-1}F$, the state equation of the FMWMP can be derived as follows

$$\begin{aligned}\dot{Z}_1 &= Z_2 \\ \dot{Z}_2 &= -f(Z_1, Z_2) + R\mathcal{J}^+(\phi)M^{-1}\tau + H.\end{aligned}\quad (12)$$

Remark 2. From (5)-(6), the values of $\dot{\theta}_i$, $i = 1, 2, 3, 4$, as well as $\text{sgn}(\dot{\theta}_i)$, $i = 1, 2, 3, 4$, are definitely up to $Z_2 = [\dot{x}_q \ \dot{y}_q \ \dot{\phi}]^T$. Thus it is reasonable to regard $R\mathcal{J}^+(\phi)M^{-1}F$ as a part of $f(Z_1, Z_2)$.

Remark 3. [41] Based on the Assumptions 1-2, the lumped disturbances/uncertainties term $H(t)$ and its time derivatives satisfy $\|H^{(j)}\| \leq \delta$, $j = 0, 1, 2, \dots, n$, where δ is also an unknown positive constant.

Remark 4. Note that in practice, the control laws are often implemented through voltage inputs regulated via PWM technique for convenience. Generally speaking, the relationship between the torque generated by the DC motor and the voltage applied to the DC motor can be roughly expressed by $\tau = \alpha u - \beta v_w$, where u is the voltage applied to the DC motor, v_w the linear velocity of the corresponding mecanum wheel, α and β are motor characteristic coefficients depending on the parameters of the DC motor that can be obtained from the its catalog or experiment [42]. Moreover, the relationship between the torque and the voltage can also be modeled in detail, which will be discussed in the Appendix.

3 Controller Design Based on ESO

To achieve accurate tracking control performance, in this section, an ESO-SMC scheme will be proposed to ensure the tracking performance based on the kinematic and dynamic models introduced in Section 2. The control structure is shown in Fig. 4.

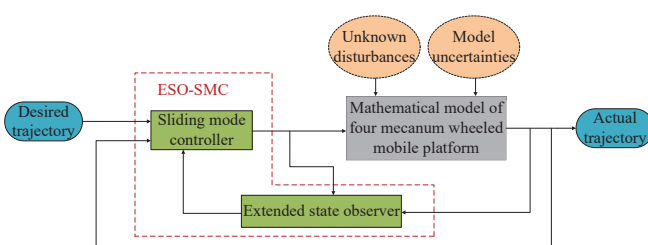


Fig. 4: Control structure of the proposed ESO-SMC scheme for FMWMP.

The control objective in this paper is to synthesize a control algorithm for $\tau_1, \tau_2, \tau_3, \tau_4$, with the unknown disturbances τ_d and model uncertainties $\Delta M, \Delta D_\theta$ and ΔF considered, such that $Z_1(t)$ tracks the reference trajectory $Z_1^d(t)$ accurately.

3.1 [43] Extended State Observer Design

In this section, an ESO will be designed to derive the unmeasurable states and the lumped disturbances/uncertainties term. The state equation of the FMWMP can be rewritten as

$$\begin{bmatrix} \dot{Z}_1 \\ \dot{Z}_2 \end{bmatrix} = \begin{bmatrix} 0_{3 \times 3} & I_{3 \times 3} \\ 0_{3 \times 3} & 0_{3 \times 3} \end{bmatrix} \begin{bmatrix} Z_1 \\ Z_2 \end{bmatrix} + \begin{bmatrix} 0_{3 \times 1} \\ R\mathcal{J}^+(\phi)M^{-1} \end{bmatrix} \tau - \begin{bmatrix} 0_{3 \times 1} \\ f(Z_1, Z_2) \end{bmatrix} + \begin{bmatrix} 0_{3 \times 1} \\ H \end{bmatrix}, \quad (13)$$

where

$$0_{3 \times 3} = \begin{bmatrix} 0 & 0 & 0 \\ 0 & 0 & 0 \\ 0 & 0 & 0 \end{bmatrix}, I_{3 \times 3} = \begin{bmatrix} 1 & 0 & 0 \\ 0 & 1 & 0 \\ 0 & 0 & 1 \end{bmatrix}.$$

Based (13), define the extended state vector as $Z = [Z_1^T \ Z_2^T \ H^T]^T = [x_q \ y_q \ \phi \ x'_q \ y'_q \ \dot{\phi} \ H_x \ H_y \ H_\phi]^T$, the lumped disturbances/uncertainties term H is defined as an extended state, and h is defined as the derivative of H . Recall that $\|h\| \leq \delta$, which has been discussed in Remark 3. Then (13) can be transformed into

$$\dot{Z} = AZ + B\tau + B_1f + B_2h, \quad (14)$$

where

$$\begin{aligned}A &= \begin{bmatrix} 0_{3 \times 3} & I_{3 \times 3} & 0_{3 \times 3} \\ 0_{3 \times 3} & 0_{3 \times 3} & I_{3 \times 3} \\ 0_{3 \times 3} & 0_{3 \times 3} & 0_{3 \times 3} \end{bmatrix} \in \mathbb{R}^{9 \times 9}, B_1 = -\begin{bmatrix} 0_{3 \times 3} \\ I_{3 \times 3} \\ 0_{3 \times 3} \end{bmatrix} \in \mathbb{R}^{9 \times 3}, \\ B &= \begin{bmatrix} 0_{3 \times 4} \\ R\mathcal{J}^+(\phi)M^{-1} \\ 0_{3 \times 4} \end{bmatrix} \in \mathbb{R}^{9 \times 4}, B_2 = \begin{bmatrix} 0_{3 \times 3} \\ 0_{3 \times 3} \\ I_{3 \times 3} \end{bmatrix} \in \mathbb{R}^{9 \times 3}.\end{aligned}$$

Then, the ESO is proposed as following form

$$\dot{\tilde{Z}} = A\tilde{Z} + B\tau + B_1\hat{f} + \alpha(Z_1 - \tilde{Z}_1), \quad (15)$$

where $\alpha = \begin{bmatrix} a_1\omega_0 I_{3 \times 3} \\ a_2\omega_0^2 I_{3 \times 3} \\ a_3\omega_0^3 I_{3 \times 3} \end{bmatrix} \in \mathbb{R}^{9 \times 9}$ is the observer gain, and ω_0 can be regarded as the bandwidth of the ESO. Define the estimation errors as follows

$$\tilde{Z} = \begin{bmatrix} \tilde{Z}_1 \\ \tilde{Z}_2 \\ \tilde{H} \end{bmatrix} = \begin{bmatrix} Z_1 - \hat{Z}_1 \\ Z_2 - \hat{Z}_2 \\ H - \hat{H} \end{bmatrix}.$$

Then the estimation error dynamic equation is given by

$$\dot{\tilde{Z}} = A\tilde{Z} + B_1\tilde{f} + B_2h - \alpha\tilde{Z}_1, \quad (16)$$

where

$$\tilde{f} = f(Z_1, Z_2) - f(\hat{Z}_1, \hat{Z}_2).$$

Define the scaled estimation as $\xi = [\xi_1 \ \xi_2 \ \xi_3]^T = [\tilde{Z}_1 \ \frac{\tilde{Z}_2}{\omega_0} \ \frac{\tilde{H}}{\omega_0^2}]^T$, then the estimation error dynamics can be transformed into

$$\dot{\xi} = \omega_0 A_\xi \xi + B_1\tilde{f}/\omega_0 + B_2h/\omega_0^2, \quad (17)$$

where

$$A_\xi = \begin{bmatrix} -a_1 I_{3 \times 3} & I_{3 \times 3} & 0_{3 \times 3} \\ -a_2 I_{3 \times 3} & 0_{3 \times 3} & I_{3 \times 3} \\ -a_3 I_{3 \times 3} & 0_{3 \times 3} & 0_{3 \times 3} \end{bmatrix} \in \mathbb{R}^{9 \times 9}.$$

Remark 5. Note that the ESO (15) proposed in this section combines the well-known HGO [44, Chapter 14.5] and ESO, i.e., the HGO is extended with a new state estimates the disturbances/uncertainties term.

Lemma 1. Considering the estimation error dynamics (17), the ESO (15) is bounded stable if only A_ξ is Hurwitz and $\omega_0 - 2\frac{\|P\|\cdot\|c_1+c_2\omega_0\|}{\omega_0} - 1 > 0$ can be satisfied.

Proof: Since matrix A_ξ is Hurwitz, there exists a matrix P which is symmetric and positive definite and it satisfies

$$A_\xi^T P + PA_\xi = I_{9 \times 9}.$$

Since $\tilde{f} = f - \hat{f}$, then according to the Lipschitz condition one can obtain that

$$\begin{aligned} \|B_1\tilde{f}\| &= \|f(Z_1, Z_2) - f(\hat{Z}_1, \hat{Z}_2)\| \leq \|c_1\hat{Z}_1 + c_2\hat{Z}_2\| \\ &\leq c_1\|\xi_1\| + c_2\omega_0\|\xi_2\| \\ &\leq (c_1 + c_2\omega_0)\|\xi\|, \end{aligned} \quad (18)$$

where c_1, c_2 are known positive constants.

Consider a Lyapunov function candidate as

$$V_1 = \xi^T P \xi, \quad (19)$$

then the time derivative of V_1 can be written as

$$\begin{aligned} \dot{V}_1 &= \dot{\xi}^T P \xi + \xi^T P \dot{\xi} \\ &= \omega_0 \xi^T A_\xi^T P \xi + \frac{(B_1 \tilde{f})^T P \xi}{\omega_0} + \frac{(B_2 h)^T P \xi}{\omega_0^2} \\ &\quad + \omega_0 \xi^T P A_\xi \xi + \frac{\xi^T P (B_1 \tilde{f})}{\omega_0} + \frac{\xi^T P (B_2 h)}{\omega_0^2} \\ &= -\omega_0 \xi^T \xi + 2 \frac{\xi^T P B_1 \tilde{f}}{\omega_0} + 2 \frac{\xi^T P B_2 h}{\omega_0^2} \\ &\leq -\left(\omega_0 - 2 \frac{\|P\| \cdot \|c_1 + c_2\omega_0\|}{\omega_0}\right) \|\xi\|^2 + 2 \frac{\xi^T P B_2 h}{\omega_0^2}. \end{aligned} \quad (20)$$

By using Young's inequality, it can be easily known that $2 \frac{\xi^T P B_2 h}{\omega_0^2} \leq \|\xi\|^2 + \frac{\|P B_2\|^2 \cdot \|h\|^2}{\omega_0^4}$. Thus one can further obtain that

$$\begin{aligned} \dot{V}_1 &\leq -\left(\omega_0 - 2 \frac{\|P\| \cdot \|c_1 + c_2\omega_0\|}{\omega_0} - 1\right) \|\xi\|^2 \\ &\quad + \frac{\|P B_2\|^2 \cdot \delta^2}{\omega_0^4}. \end{aligned} \quad (21)$$

Since the values of $\|P B_2\|$ and ω_0 are depending on the design parameters and δ is a bounded positive constant, the part $\frac{\|P B_2\|^2 \cdot \delta^2}{\omega_0^4}$ in (21) is a bounded positive constant. It can be concluded that the proposed ESO is bounded stable if only the parameters satisfy $\omega_0 - 2 \frac{\|P\| \cdot \|c_1 + c_2\omega_0\|}{\omega_0} - 1 > 0$. This ends the proof. \square

3.2 [35] Sliding Mode Controller Design

In order to guarantee a satisfied tracking performance for the FMWMP, an ESO based SMC controller will be proposed in this section.

Define $e = Z_1 - Z_1^d$ as the tracking error, where Z_1^d represents the desired trajectory. Then the sliding surface is designed as

$$s(t) = \lambda e(t) + \dot{e}(t), \quad (22)$$

where λ is a designed positive definite diagonal matrix. Employing the time derivative one can obtain that

$$\begin{aligned} \dot{s}(t) &= \lambda \dot{e}(t) + \ddot{e}(t) \\ &= \lambda (\hat{Z}_2 - \hat{Z}_1^d) + (\dot{\hat{Z}}_2 - \dot{\hat{Z}}_1^d) \\ &= \lambda (\hat{Z}_2 - \hat{Z}_1^d) + [-\hat{f} + R J^+(\phi) M^{-1} \tau + \hat{H} - \ddot{Z}_1^d]. \end{aligned} \quad (23)$$

Thus the reaching control law is obtained as

$$\tau_r(t) = \frac{1}{R} M J(\phi) [\hat{f} - \hat{H} + \ddot{Z}_1^d - \lambda (\hat{Z}_2 - \hat{Z}_1^d)]. \quad (24)$$

Design the switching control law as

$$\tau_{sw}(t) = \frac{1}{R} M J(\phi) [-k_1 s(t) - k_2 \operatorname{sgn}(s(t))], \quad (25)$$

where k_1, k_2 is the positive definite switching gain matrices. Hence, the total input torque vector can be obtained

$$\begin{aligned} \tau(t) &= \tau_r(t) + \tau_{sw}(t) \\ &= \frac{1}{R} M J(\phi) [\hat{f} - \hat{H} + \ddot{Z}_1^d - \lambda (\hat{Z}_2 - \hat{Z}_1^d) \\ &\quad - k_1 s(t) - k_2 \operatorname{sgn}(s(t))]. \end{aligned} \quad (26)$$

Lemma 2. ([45]) Let function $V(t) \geq 0$ be a continuous function defined $\forall t \geq 0$ and bounded, and $\dot{V}(t) \leq -\rho V(t) + \kappa$, where ρ and κ are positive constants, then

$$V(t) \leq V(0) e^{-\rho t} + \frac{\kappa}{\rho} (1 - e^{-\kappa t}).$$

Theorem 1. Considering the uncertain system (11), with the designed ESO (15) and the SMC controller (26). The estimation errors of proposed ESO and the FMWMP tracking errors will be guaranteed to be UUB.

Proof: Consider a Lyapunov function candidate as

$$V = \frac{1}{2} \xi^T P \xi + \frac{1}{2} s^T s. \quad (27)$$

According to (21)-(26), one can obtain that

$$\begin{aligned} \dot{V} &\leq -\frac{1}{2} \left(\omega_0 - 2 \frac{\|P\| \cdot \|c_1 + c_2\omega_0\|}{\omega_0} - 1 \right) \|\xi\|^2 \\ &\quad + \frac{\|P B_2\|^2 \cdot \delta^2}{2\omega_0^4} + s^T (-k_1 s - k_2 \operatorname{sgn}(s)) \\ &\leq -\frac{1}{2} \left(\omega_0 - 2 \frac{\|P\| \cdot \|c_1 + c_2\omega_0\|}{\omega_0} - 1 \right) \|\xi\|^2 \\ &\quad - \lambda_{min}(k_1) \|s\|^2 - \lambda_{min}(k_2) \|s\| + \frac{\|P B_2\|^2 \cdot \delta^2}{2\omega_0^4} \\ &\leq -\eta^T \Lambda \eta + \zeta, \end{aligned} \quad (28)$$

where

$$\eta = [\xi^T, s^T]^T \in \mathbb{R}^{6 \times 1}, \quad \Lambda = \begin{bmatrix} \Lambda_1 & 0_{3 \times 3} \\ 0_{3 \times 3} & \Lambda_2 \end{bmatrix} \in \mathbb{R}^{6 \times 6}, \quad \zeta = \frac{\|P B_2\|^2 \cdot \delta^2}{2\omega_0^4} - \lambda_{min}(k_2) \|s\|. \text{ In which } \Lambda_1 = \operatorname{diag}\{\chi, \chi, \chi\}, \text{ with}$$

$\chi = \frac{1}{2}(\omega_0 - 1 - 2\frac{\|P\|\cdot\|c_1+c_2\omega_0\|}{\omega_0})$, $\Lambda_2 = \text{diag}\{\varsigma, \varsigma, \varsigma\}$, with $\varsigma = \lambda_{\min}(k_1)$. According to **lemma 1**, Λ_1 and Λ_2 are positive definite matrices, thus it satisfies that

$$\begin{aligned}\dot{V} &\leq -\lambda_{\min}(\Lambda)(\|\xi\|^2 + \|s\|^2) + \zeta \\ &\leq -\lambda_{\min}(\Lambda) \left(\frac{1}{\lambda_{\max}(P)} \xi^T P \xi + s^T s \right) + \zeta \\ &\leq -\gamma V + \zeta,\end{aligned}\quad (29)$$

where $\gamma = 2\lambda_{\min}(\Lambda)\min\left\{1, \frac{1}{\lambda_{\max}(P)}\right\}$. Then based on **Lemma 2**, it can be obtained that

$$V(t) \leq V(0)e^{-\gamma t} + \frac{\zeta}{\gamma}(1 - e^{-\gamma t}). \quad (30)$$

Recall (27) it is known that $V(t) \geq \frac{1}{2}\xi^T P \xi \geq \frac{1}{2}\lambda_{\min}(P)\|\xi\|^2$, it satisfied that

$$\frac{1}{2}\lambda_{\min}(P)\|\xi\|^2 \leq V(0)e^{-\gamma t} + \frac{\zeta}{\gamma}(1 - e^{-\gamma t}). \quad (31)$$

$$\|\xi\| \leq \sqrt{\frac{2(V(0)\gamma e^{-\gamma t} + \zeta(1 - e^{-\gamma t}))}{\gamma\lambda_{\min}(P)}} < \sqrt{\frac{2(V(0)\gamma + \zeta)}{\gamma\lambda_{\min}(P)}}. \quad (32)$$

$$\|\xi\| \leq \sqrt{\frac{2\zeta}{\gamma\lambda_{\min}(P)}}, \quad t \rightarrow \infty. \quad (33)$$

Similarly, $V(t) \geq \frac{1}{2}s^T s = \frac{1}{2}\|s\|^2$, then

$$\|s\| \leq \sqrt{\frac{2(V(0)\gamma e^{-\gamma t} + \zeta(1 - e^{-\gamma t}))}{\gamma}} < \sqrt{\frac{2(V(0)\gamma + \zeta)}{\gamma}}. \quad (34)$$

$$\|s\| \leq \sqrt{\frac{2\zeta}{\gamma}}, \quad t \rightarrow \infty. \quad (35)$$

Thus, all signals of the closed-loop system, i.e., ξ and s , are UUB. As a result, the tracking error e will be attracted into a small stable region contain the origin by appropriately selecting parameters [46]. This completes the proof. \square

4 Numerical Simulations

As the capability to track the desired trajectory accurately in face of the UDMU of FMWMP has been presented in Section 3 through Lyapunov analysis, to further verify that, in this section, a numerical example of FMWMP will be used to perform simulations through Matlab/Simulink.

To illustrate the robustness of proposed controller for different trajectories, simulations are carried out with two different reference trajectories: one is circle reference trajectory and the other is lemniscate reference trajectory. It is worth to note that these two trajectories are typical ones, i.e., the former one has the constant curvature and the latter one has the time-variant curvature. The trajectories are set as:

1) Circle reference trajectory

$$Z_1^d(t) = \begin{bmatrix} x_d(t) \\ y_d(t) \\ \phi_d(t) \end{bmatrix} = \begin{bmatrix} 3 \sin(0.1t) m \\ 3 \cos(0.1t) m \\ \frac{\pi}{2} \sin(0.1t) rad \end{bmatrix}. \quad (36)$$

2) Lemniscate reference trajectory

$$Z_1^d(t) = \begin{bmatrix} x_d(t) \\ y_d(t) \\ \phi_d(t) \end{bmatrix} = \begin{bmatrix} 5 \cos(0.1t) m \\ 2.5 \sin(0.2t) m \\ \frac{\pi}{2} \sin(0.1t) rad \end{bmatrix}. \quad (37)$$

The lumped uncertainties are assumed as $H = [0.5e^{-0.02t} \cos(t) \ 0.2 \sin(t) \ 0.5 \cos(t)]^T$. Parameter selections of the FMWMP and the controller of the simulations are listed in Table 2.

The ESO performance is shown in Figs. 5, 6, 9 and 10. In Figs. 5 and 9, the estimation errors of \dot{x}_q , \dot{y}_q and $\dot{\phi}$ are presented respectively. While in Figs. 5 and 9, the estimation errors of H_x , H_y and H_ϕ are shown respectively. It can be observed that for two different reference trajectories, the convergence time is less than 0.03s both in the estimation of Z_2 and H . It demonstrates that the proposed ESO generates good performance with fast convergence and small-enough steady-state errors.

Figs. 7 and 11 show the trajectory tracking performance of the controller designed in Section 3. Three curves are plotted as tracking errors of x_q , y_q and ϕ , respectively. It's obviously that the proposed ESO-SMC strategy can drive the FMWMP to the desired trajectory, not only with the circle reference trajectory, but also with the lemniscate reference trajectory, which verifies the closed-loop stability.

Figs. 8 and 12 illustrate the control inputs of the four DC motors. It can be seen that all the control inputs are continuous and varying between -20N·m and 20N·m. One can conclude that the magnitude of control commands of DC motors are always within a given range as expected.

5 Experiments and Comparisons

To further validate the effectiveness of proposed ESO-SMC strategy from a practical perspective, experimental studies will be developed via a FMWMP in this section, followed by the performance comparisons between ESO-SMC controller and PID controller.

Table 2 Parameters of ESO-SMC of simulations

Parameter	Value(Unit)	Parameter	Value(Unit)
a	$0.35(m)$	a_1	6
b	$0.25(m)$	a_2	11
m	$8(kg)$	a_3	6
R	$0.05(m)$	ω_0	200
J_ω	$0.2(N\cdot m)$	λ	$\text{diag}\{0.9, 0.9, 0.8\}$
J_z	$0.1(N\cdot m)$	k_1	$\text{diag}\{0.18, 0.15, 0.07\}$
f_i	$10(N)$	k_2	$\text{diag}\{0.18, 0.1, 0.08\}$
D_θ	0.2		

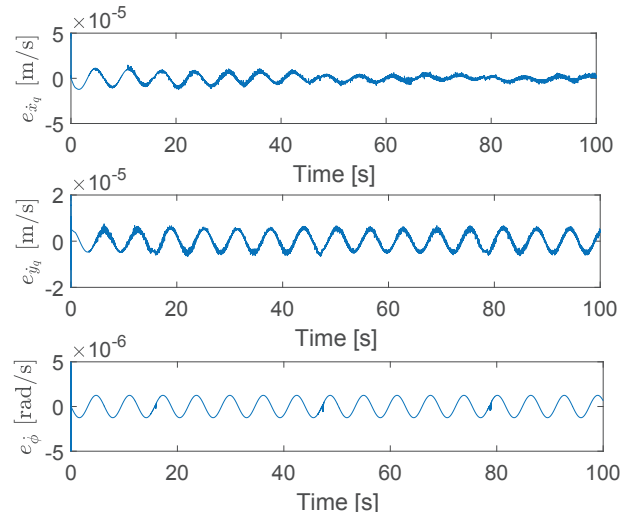


Fig. 5: Estimation errors of Z_2 with circle reference trajectory.

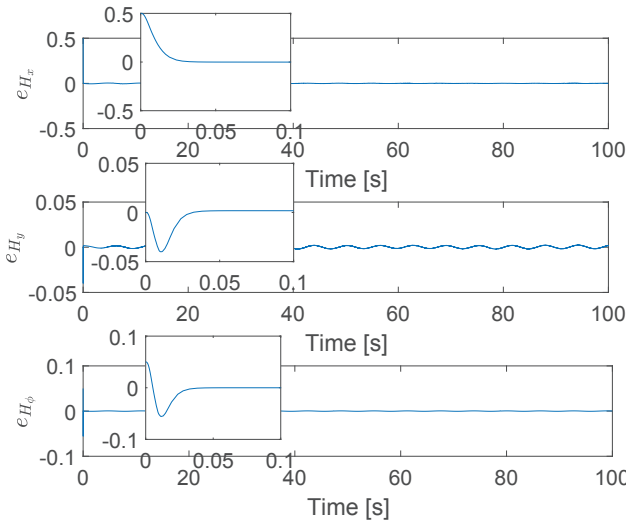


Fig. 6: Estimation errors of H with circle reference trajectory.

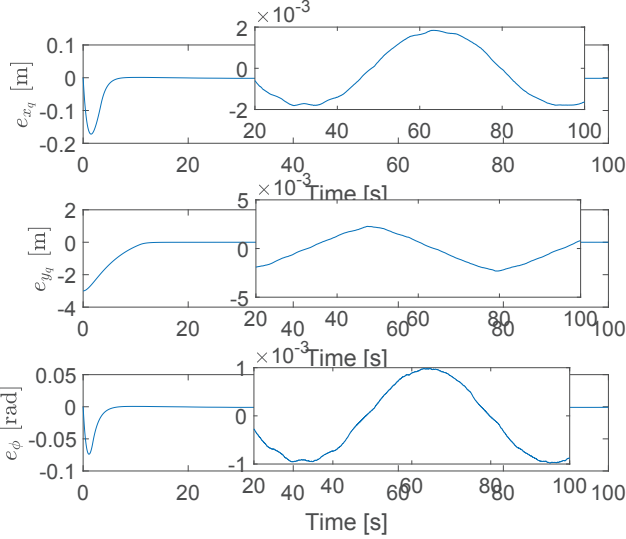


Fig. 7: Tracking errors of Z_1 with circle reference trajectory.

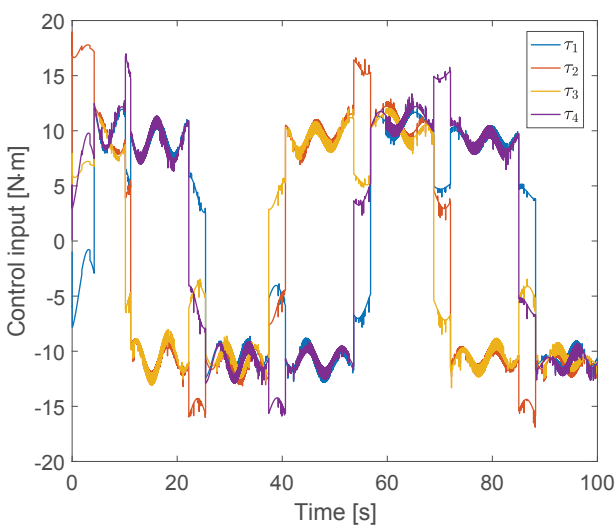


Fig. 8: Control inputs with circle reference trajectory.

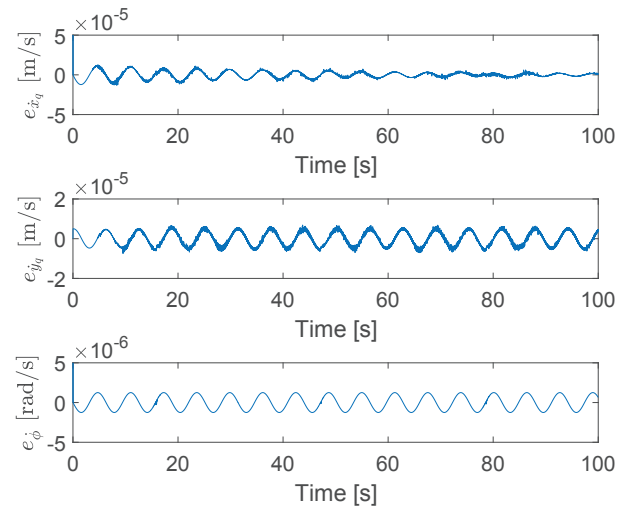


Fig. 9: Estimation errors of Z_2 with lemniscate reference trajectory.

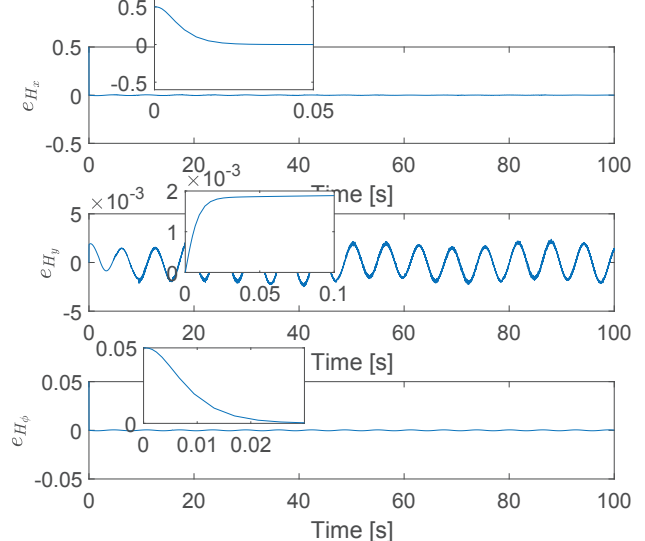


Fig. 10: Estimation errors of H with lemniscate reference trajectory.

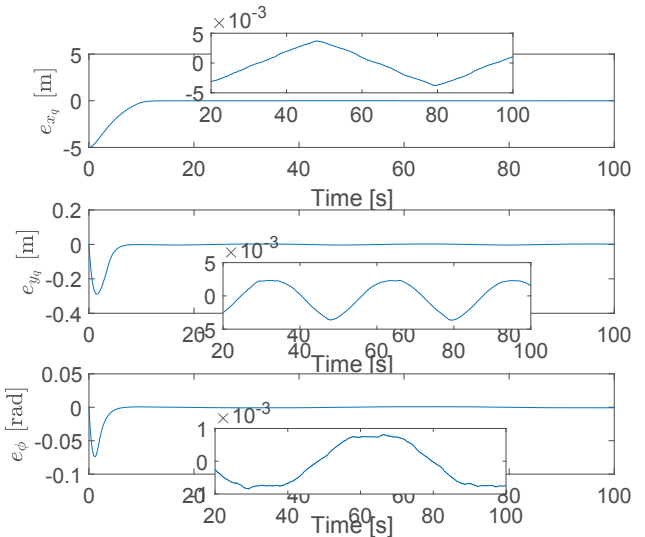


Fig. 11: Tracking Errors of Z_1 with lemniscate reference trajectory.

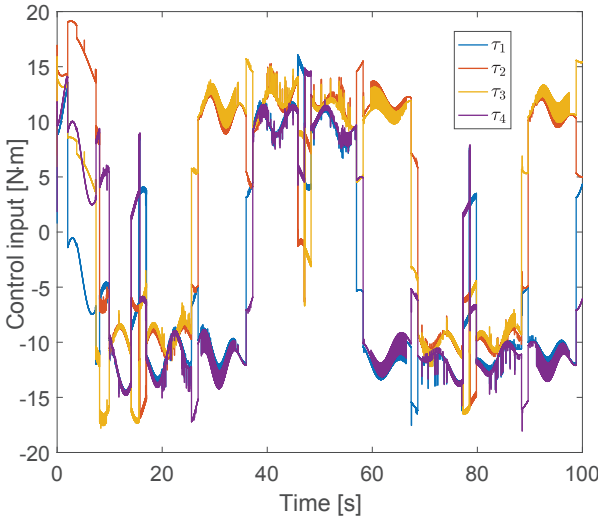


Fig. 12: Control inputs with lemniscate reference trajectory.

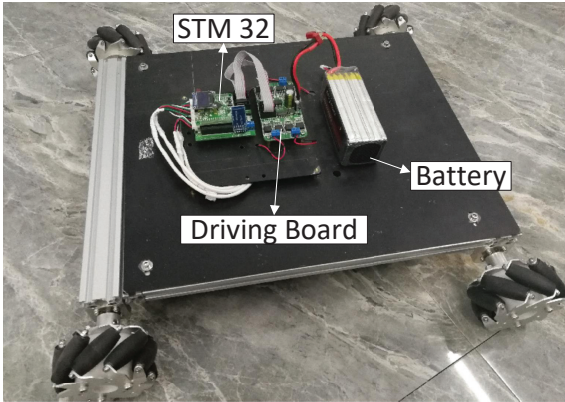


Fig. 13: The FMWMP used for experiments.

5.1 Experiment Setup

The FMWMP used for the experiments is shown in Fig. 13. It includes four mecanum wheels which generated by four separated DC motors, a STM32 chip, and a driving board. To measure the (x-y) position and rotation information, an Ultra-wideband (UWB) positioning system is built and an Inertial measurement unit (IMU) is settled on STM32 chip, respectively. UWB positioning system is one kind of high-precision in-door locating technology which consists four anchors whose positions are known. The position of FMWMP is obtained through the different distances between the FMWMP and four anchors. Compared with other positioning methods such as Bluetooth based and Wi-Fi based positioning systems, the UWB positioning system is more suitable for real-time locating due to its shorter communication time. The compute unit adopted in our experiments is a NVIDIA's Jetson TX2, which has 64-bit Denver 2 and A57 CPUs with 8 GB RAM. Note that the output voltage of the battery in experiments is less than 25.2 V. The sample rate in this experimental situation is 200 Hz. The signal flow of the FMWMP control is shown in Fig. 14.

To show the ability for tracking different trajectories of the FMWMP, two experiments were given for the FMWMP, similar to the simulations, one is with the circle reference trajectory and the other is with the lemniscate reference. The trajectories are set as:

1) Circle reference trajectory

$$Z_1^d(t) = \begin{bmatrix} x_d(t) \\ y_d(t) \\ \phi_d(t) \end{bmatrix} = \begin{bmatrix} 3 \sin(0.1t) m \\ 3 \cos(0.1t) m \\ \frac{\pi}{2} \sin(0.1t) rad \end{bmatrix}. \quad (38)$$

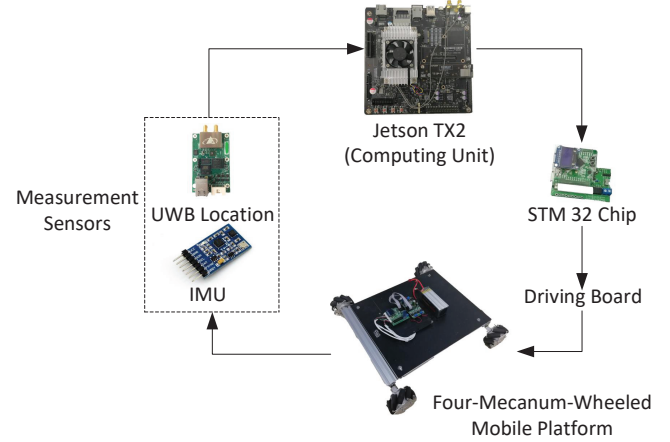


Fig. 14: Signal flow of the FMWMP control.

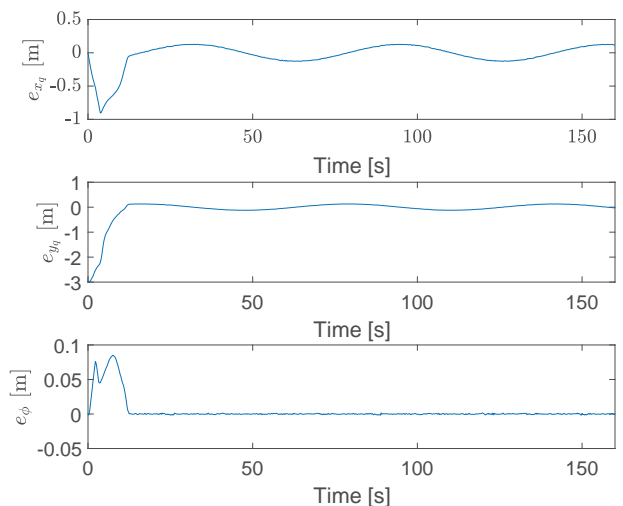


Fig. 15: Tracking errors of Z_1 with circle reference trajectory.

2) Lemniscate reference trajectory

$$Z_1^d(t) = \begin{bmatrix} x_d(t) \\ y_d(t) \\ \phi_d(t) \end{bmatrix} = \begin{bmatrix} 5 \cos(0.1t) m \\ 2.5 \sin(0.2t) m \\ \frac{\pi}{2} \sin(0.1t) rad \end{bmatrix}. \quad (39)$$

5.2 Experimental Results

Experimental results are shown in Figs. 15-18 and Figs. 19-22 for circle reference trajectory and lemniscate reference trajectory, respectively. For case 1), Fig. 15 shows the tracking errors in experiment. It can be noticed that errors converge to zero quickly and the steady-state errors are bounded and small-enough. Fig. 16 presents the estimation results of the lumped disturbances/uncertainties term H . Fig. 17 illustrates the control inputs of four DC motors, it can be seen that the control inputs are always within the expect range. In Fig. 18, graphics of the reference trajectory and the actual trajectory are also plotted as functions of time. For case 2), similar to case 1), Figs. 19-22 show the experimental results for lemniscate curve reference trajectory, also indicate that the proposed controller have a good tracking performance. It is shown that the proposed ESO-SMC scheme has both the good tracking performance and robustness.

It is worth to mention that in Figs. 15 and 19, peaking phenomenon appears, which is caused by different initial values of the ESO. This kind of phenomenon sometimes may lead the ESO even the plant to be unstable if the peaking values go too large. Some

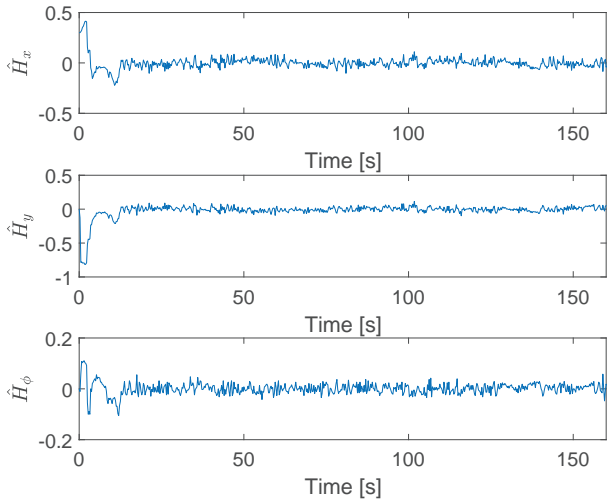


Fig. 16: Estimation values of H with circle reference trajectory.

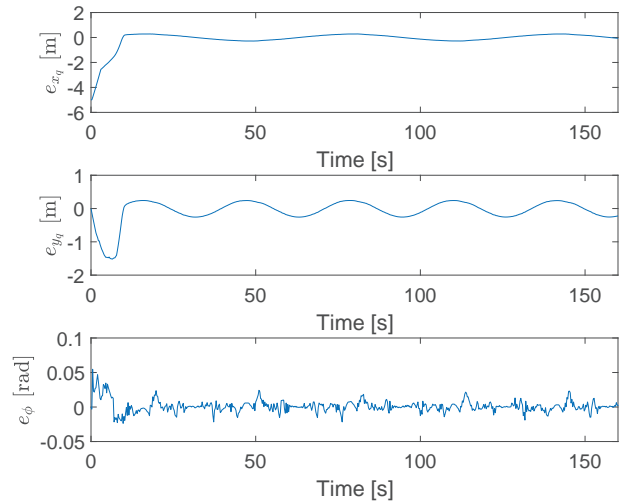


Fig. 19: Tracking errors of Z_1 with lemniscate reference trajectory.

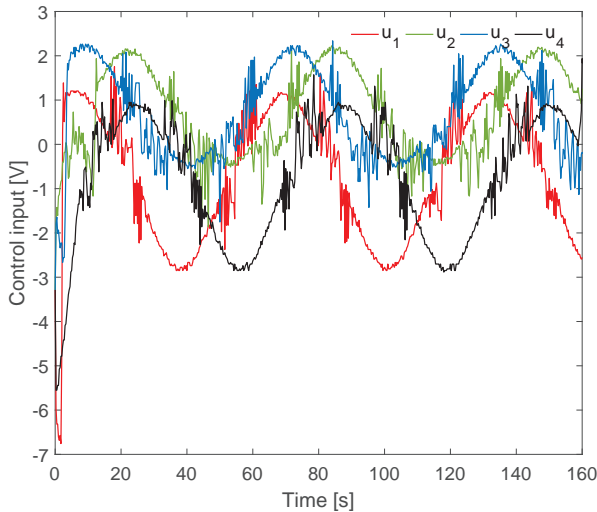


Fig. 17: Control inputs with circle reference trajectory.

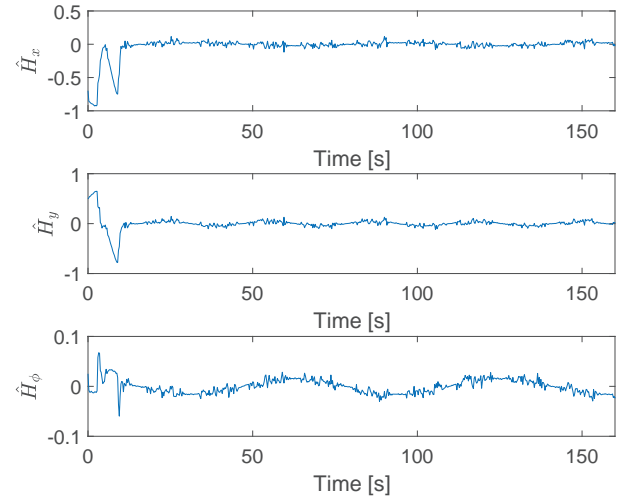


Fig. 20: Estimation values of H with lemniscate reference.

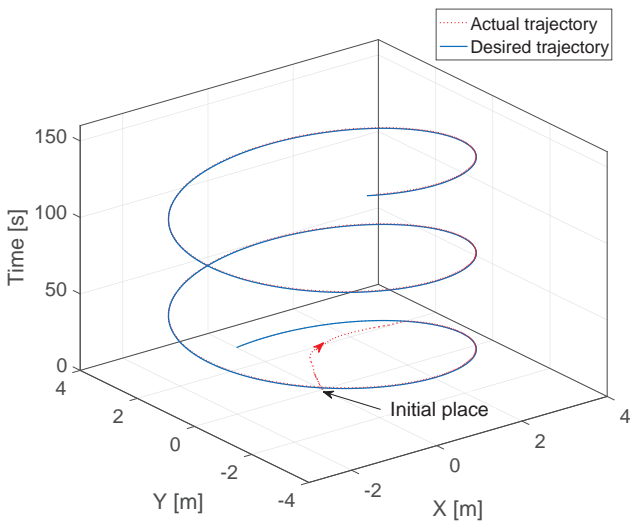


Fig. 18: Tracking trajectory with circle reference trajectory.

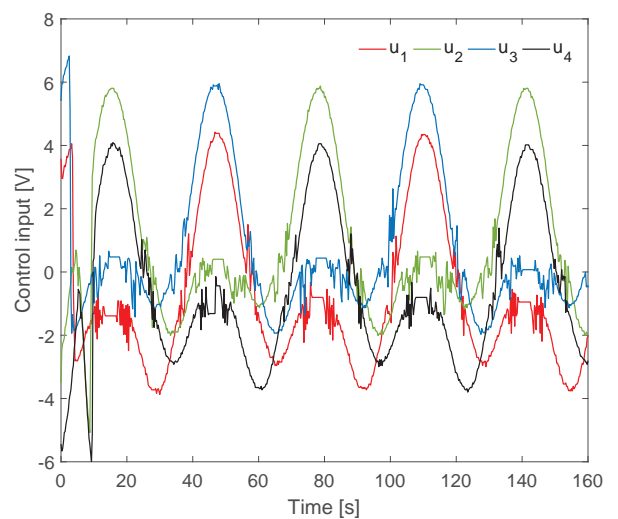


Fig. 21: Control inputs with lemniscate reference trajectory.

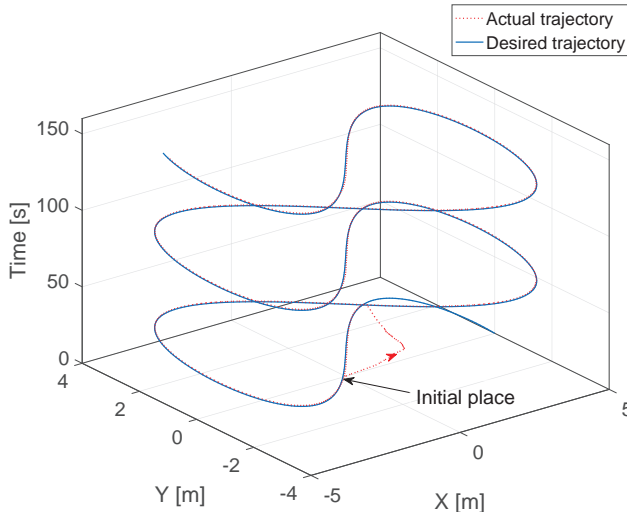


Fig. 22: Tracking trajectory with lemniscate reference trajectory.

approaches to alleviate the peaking phenomenon have been proposed in the previous literatures [47, 48]. In [47], a globally bounded state feedback control law is designed. During the short transient period when the state estimates exhibit peaking, the controller saturates, thus preventing peaking from being transmitted to the plant. In [?], the bandwidth ω_0 is designed as a time-increasing function during the initial period, i.e.,

$$\omega_0 = \begin{cases} 200(\frac{t}{10})^3 & 0 \leq t \leq 10 \\ 200 & t > 10. \end{cases}$$

Recall that $Z_2(0) - \hat{Z}_2(0) = \omega_0 \xi_2$ and $H(0) - \hat{H}(0) = \omega_0^2 \xi_3$. With this approach, the values of $Z_2(0) - \hat{Z}_2(0)$ and $H(0) - \hat{H}(0)$ will not go very large and thus the peaking phenomenon can be removed. However, it should be mentioned that all the aforementioned approaches may slow down the converge rate of the plant. Therefore, in practice, the controller should be designed in accordance of both two conflictive aspects, i.e., avoid peaking phenomenon and achieve quick response.

It can be observed in Figs. 17 and 21, the chattering phenomenon is obvious when the input voltages are small. The reason is that when the command voltage applied to a DC motor is small, the DC motor enters the low-speed region. It is known that DC motor can not generate torque large enough as expected in the low-speed region. In consequence, the tracking errors would increase, which causes the increase of input voltage. Then the DC motor leaves the low-speed region. However, at this moment, the actual input voltage is larger than the command input voltage and therefore the DC motor generates larger torque than expected. In consequence, the tracking errors would increase again which causes the decrease of input voltage. Therefore, when the command control inputs are small, as the process mentioned above takes place repeatedly, the actual input voltages switch fast and there comes the chattering.

5.3 Performance Comparisons

In this section, the tracking performance between ESO-SMC controller and PID controller of FMWMP will be compared.

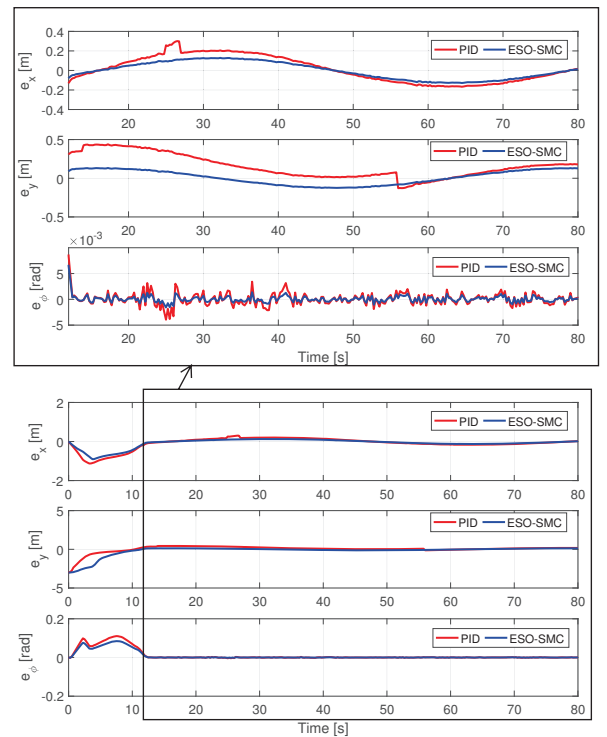


Fig. 23: Comparisons of tracking performance with circle reference trajectory.

The PID controller is designed as follows

$$\begin{aligned} U_1 &= K_{p1}\Delta_1 + K_{i1} \int \Delta_1 + K_{d1} \frac{d\Delta_1}{dt}, \\ U_2 &= K_{p2}\Delta_2 + K_{i2} \int \Delta_2 + K_{d2} \frac{d\Delta_2}{dt}, \\ U_3 &= K_{p3}\Delta_3 + K_{i3} \int \Delta_3 + K_{d3} \frac{d\Delta_3}{dt}, \\ U_4 &= K_{p4}\Delta_4 + K_{i4} \int \Delta_4 + K_{d4} \frac{d\Delta_4}{dt}, \end{aligned} \quad (40)$$

where

$$\begin{aligned} \Delta_1 &= -(x_d - x) + (y_d - y) - (\phi_d - \phi)(a + b), \\ \Delta_2 &= (x_d - x) + (y_d - y) - (\phi_d - \phi)(a + b), \\ \Delta_3 &= -(x_d - x) + (y_d - y) + (\phi_d - \phi)(a + b), \\ \Delta_4 &= (x_d - x) + (y_d - y) + (\phi_d - \phi)(a + b). \end{aligned} \quad (41)$$

To illustrate the steady state tracking errors in a quantitative way, the following indices are used to evaluate steady-state tracking performance:

$$\|e\|_{RMS} = \sqrt{\frac{1}{N} \sum_{i=1}^N \|e\|^2},$$

where N equals to the sampling steps. As illustrated in Figs. 23 and 24, the tracking errors enter the steady state after 12s with circle reference, and 10s with lemniscate reference. The values $\|e_x\|_{RMS}$, $\|e_y\|_{RMS}$ and $\|e_\phi\|_{RMS}$ with the circle reference and the lemniscate reference are shown in Table 3 and Table 4, respectively.

Comparative results in Table 3 and Table 4 indicate that after the FMWMP system enters the steady state, i.e., after the FMWMP system breaks away from the impact region of the peak overshoots, the proposed ESO-SMC controller has higher tracking accuracy than

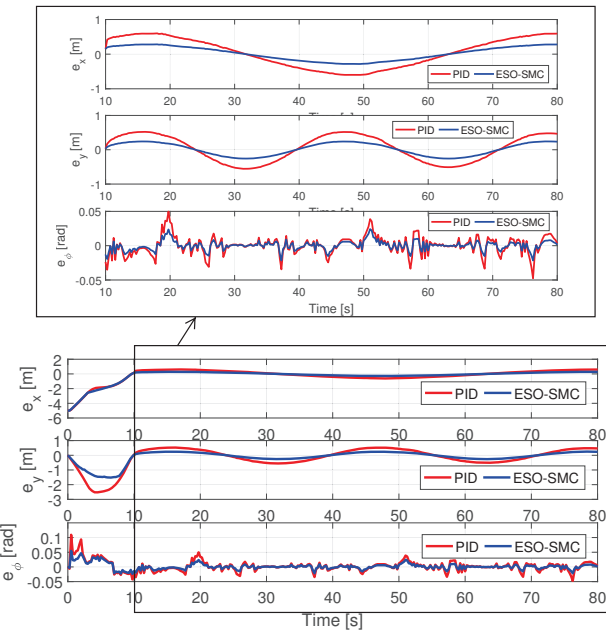


Fig. 24: Comparisons of tracking performance with lemniscate reference trajectory.

PID controller. The performance of ESO-SMC controller has an obvious improvement compared with PID controller.

Note that there are two main aspects influencing on the tracking performance.

(1) The four mecanum wheeled mobile platform (FMWMP) used in the experiment has four DC motors with different characteristics, such as respond time, dead-zone, which degrades the tracking performance. Moreover, the chattering induced by the DC motors in case that the control inputs are small (DC motor enters low-speed region) also brings influences on the tracking performance.

(2) It is noted that mecanum wheel suffers slippage more frequently compared than common wheel [49]. As [49] concerns, the main sources of position errors are the slippage between the mecanum wheel and the floor surface. Hence the slippage also influences on the tracking performance.

Generally speaking, when a FMWMP is tracking circle or lemniscate trajectory, the DC motors need change their rotation directions frequently and therefore often work in low-speed region. Moreover, since both circle and lemniscate trajectories are curves, the slippage may appear almost all the time. Thus, the RMS errors in Tables 3 and 4 are acceptable in practice. It would be difficult to implement errors

Table 3 RMS values of tracking error with circle reference trajectory

RMS value	PID(Unit)	ESO-SMC(Unit)	Improvement
$\ e_{xq}\ _{RMS}$	0.1213(m)	0.0876(m)	27.8%
$\ e_{yq}\ _{RMS}$	0.1397(m)	0.0907(m)	35.1%
$\ e_\phi\ _{RMS}$	0.0011(rad)	0.0005(rad)	54.5%

Table 4 RMS values of tracking error with lemniscate reference trajectory

RMS value	PID(Unit)	ESO-SMC(Unit)	Improvement
$\ e_{xq}\ _{RMS}$	0.4191(m)	0.1979(m)	52.8%
$\ e_{yq}\ _{RMS}$	0.3784(m)	0.1805(m)	52.3%
$\ e_\phi\ _{RMS}$	0.0131(rad)	0.0068(rad)	48.1%

reduction since the aforementioned reasons are inherent characteristics of mecanum wheel and DC motor. In practical application, the trajectory for which a FMWMP tracking should be planned with slowly varying curvature as far as possible so that the two sources of tracking error mentioned above can be reduced as far as possible.

6 Conclusion

This paper concerns about the tracking control problems of a FMWMP in face of the UDMU. To overcome the control challenges, we propose an ESO to estimate the unmeasurable states and the lumped disturbances/uncertainties term, based on which a SMC scheme is applied. Simulations show that the proposed ESO has a good estimation performance. To further validate the effectiveness of proposed method, two experiments are given to demonstrate the ability of proposed method for tracking different trajectories. The experimental results illustrate that the proposed ESO-SMC scheme can drive the FMWMP to the desired trajectory with the steady state tracking errors bounded. Also, comparative studies indicate that ESO-SMC controller has better tracking performance than PID controller.

7 Acknowledgments

This work was supported in part by the National Natural Science Foundation of China (61525303, 41772377 and 61673130), the Top-Notch Young Talents Program of China (Ligang Wu), and the Self-Planned Task of State Key Laboratory of Robotics and System (HIT)(SKLRS201806B).

8 References

- M. Chen, "Disturbance attenuation tracking control for wheeled mobile robots with skidding and slipping," *IEEE Trans. Ind. Electron.*, vol. 64, no. 4, pp. 3359–3368, Apr. 2017.
- X. Liang, H. Wang, Y. H. Liu, W. Chen, and T. Liu, "Formation control of nonholonomic mobile robots without position and velocity measurements," *IEEE Trans. Robot.*, vol. 34, no. 2, pp. 434–446, Apr. 2018.
- H. Yang, M. Guo, Y. Xia, and L. Cheng, "Trajectory tracking for wheeled mobile robots via model predictive control with softening constraints," *IET Control Theory Appl.*, vol. 12, no. 2, pp. 206–214, 30 1 2018.
- K. Shojaei and A. M. Shahri, "Output feedback tracking control of uncertain non-holonomic wheeled mobile robots: a dynamic surface control approach," *IET Control Theory Appl.*, vol. 6, no. 2, pp. 216–228, Jan. 2012.
- D. Rotondo, V. Puig, F. Nejjari, and J. Romera, "A fault-hiding approach for the switching quasi-lpv fault-tolerant control of a four-wheeled omnidirectional mobile robot," *IEEE Trans. Ind. Electron.*, vol. 62, no. 6, pp. 3932–3944, Jun. 2015.
- D. Xu, D. Zhao, J. Yi, and X. Tan, "Trajectory tracking control of omnidirectional wheeled mobile manipulators: Robust neural network-based sliding mode approach," *IEEE Trans. Syst., Man, Cybern. B, Cybern.*, vol. 39, no. 3, pp. 788–799, Jun. 2009.
- J. Huang, T. V. Hung, and M. Tseng, "Smooth switching robust adaptive control for omnidirectional mobile robots," *IEEE Trans. Control Syst. Technol.*, vol. 23, no. 5, pp. 1986–1993, Sep. 2015.
- V. Andaluz, F. Roberti, J. M. Toibero, and R. Carelli, "Adaptive unified motion control of mobile manipulators," *Control Eng. Pract.*, vol. 20, no. 12, pp. 1337–1352, Dec. 2012.
- R. C. Luo and Y. Tsai, "On-line adaptive control for minimizing slippage error while mobile platform and manipulator operate simultaneously for robotics mobile manipulation," *41st Annual Conf. of the IEEE Ind. Electron. Society*, pp. 679–684, Nov. 2015.
- A. Pepe, D. Chiaravallii, and C. Melchiorri, "A hybrid teleoperation control scheme for a single-arm mobile manipulator with omnidirectional wheels," *IEEE/RSJ Int. Conf. Intell. Robot. and Syst.*, pp. 1450–1455, Oct. 2016.
- S. Kim and S. Kwon, "Nonlinear optimal control design for underactuated two-wheeled inverted pendulum mobile platform," *IEEE/ASME Trans. Mechatronics*, vol. 22, no. 6, pp. 2803–2808, Dec. 2017.
- P. Vlantis, C. P. Bechlioulis, G. Karraas, G. Fournas, and K. J. Kyriakopoulos, "Fault tolerant control for omni-directional mobile platforms with 4 mecanum wheels," *IEEE Int. Conf. Robot. and Autom.*, pp. 2395–2400, May. 2016.
- H. C. Huang, "A hybrid metaheuristic embedded system for intelligent vehicles using hypermutated firefly algorithm optimized radial basis function neural network," *IEEE Trans. Ind. Informat.*, to be published, DOI 10.1109/TII.2018.2796556.
- V. Alakshendra and S. S. Chiddarwar, "A robust adaptive control of mecanum wheel mobile robot: simulation and experimental validation," *IEEE/RSJ Int. Conf. Intell. Robot. and Syst.*, pp. 5606–5611, Oct. 2016.

- 15 C. Tsai and H. Wu, "Nonsingular terminal sliding control using fuzzy wavelet networks for mecanum wheeled omni-directional vehicles," *Int. Conf. Fuzzy Syst.*, pp. 1–6, Jul. 2010.
- 16 C. Tsai, H. Wu, F. Tai, and Y. Chen, "Adaptive backstepping decentralized formation control using fuzzy wavelet neural networks for uncertain mecanum-wheeled omnidirectional multi-vehicles," *IEEE Int. Conf. Ind. Technol.*, pp. 1446–1451, Mar. 2016.
- 17 V. Alakshendra and S. S. Chiddarwar, "Adaptive robust control of mecanum-wheeled mobile robot with uncertainties," *Nonlinear Dyn.*, vol. 87, no. 4, pp. 2147–2169, 2017.
- 18 G. Sun, Z. Ma, and J. Yu, "Discrete-Time Fractional Order Terminal Sliding Mode Tracking Control for Linear Motor," *IEEE Trans. Ind. Electron.*, vol. 65, no. 4, pp. 3386–3394, Apr. 2018.
- 19 Y. Niu, J. Lam and X. Wang, "Sliding-mode control for uncertain neutral delay systems," *IEE Proc. - Control Theory Appl.*, vol. 151, no. 1, pp. 38–44, Jan. 2004.
- 20 L. Wu, Y. Gao, J. Liu, and H. Li, "Event-triggered sliding mode control of stochastic systems via output feedback," *Automatica*, vol. 82, pp. 79–92, Aug. 2017.
- 21 Y. Zhao, J. Wang, F. Yan, and Y. Shen, "Adaptive sliding mode fault-tolerant control for type-2 fuzzy systems with distributed delays," *Inform. Sciences*, vol. 473, pp. 227–238, Jan. 2019.
- 22 F.-J. Lin and S.-L. Chiou, "Adaptive fuzzy sliding-mode control for PM synchronous servo motor drives," *IEE Proc. - Control Theory Appl.*, vol. 145, no. 1, pp. 63–72, Jan. 1998.
- 23 G. Sun, L. Wu, Z. Kuang, Z. Ma, and J. Liu, "Practical tracking control of linear motor via fractional-order sliding mode," *Automatica*, vol. 94, pp. 221–235, Aug. 2018.
- 24 A. J. Koshkouei, K. J. Burnham, and A. S. I. Zinober, "Dynamic sliding mode control design," *IEE Proc. - Control Theory Appl.*, vol. 152, no. 4, pp. 392–396, Jul. 2005.
- 25 B. S. Park, S. J. Yoo, J. B. Park, and Y. H. Choi, "Adaptive neural sliding mode control of nonholonomic wheeled mobile robots with model uncertainty," *IEEE Trans. Control Syst. Technol.*, vol. 17, no. 1, pp. 207–214, Jan. 2009.
- 26 M. Defoort, T. Floquet, A. Kokosy, and W. Perruquetti, "Sliding-mode formation control for cooperative autonomous mobile robots," *IEEE Trans. Ind. Electron.*, vol. 55, no. 11, pp. 3944–3953, Nov. 2008.
- 27 A. Ferrara and M. Rubagotti, "Second-order sliding-mode control of a mobile robot based on a harmonic potential field," *IET Control Theory Appl.*, vol. 2, no. 9, pp. 807–818, Sep. 2008.
- 28 G. P. Incremona, M. Rubagotti, and A. Ferrara, "Sliding mode control of constrained nonlinear systems," *IEEE Trans. Autom. Control*, vol. 62, no. 6, pp. 2965–2972, Jun. 2017.
- 29 G. Bartolini, A. Ferrara, and E. Usai, "Chattering avoidance by second-order sliding mode control," *IEEE Trans. Autom. Control*, vol. 43, no. 2, pp. 241–246, Feb. 1998.
- 30 J. Baek, M. Jin, and S. Han, "A new adaptive sliding-mode control scheme for application to robot manipulators," *IEEE Trans. Ind. Electron.*, vol. 63, no. 6, pp. 3628–3637, Jun. 2016.
- 31 J. Yang, S. Li, and X. Yu, "Sliding-mode control for systems with mismatched uncertainties via a disturbance observer," *IEEE Trans. Ind. Electron.*, vol. 60, no. 1, pp. 160–169, Jan. 2013.
- 32 D. Won, W. Kim, D. Shin, and C. C. Chung, "High-Gain Disturbance Observer-Based Backstepping Control With Output Tracking Error Constraint for Electro-Hydraulic Systems," *IEEE Trans. Control Syst. Technol.*, vol. 23, no. 2, pp. 787–795, Mar. 2015.
- 33 K. D. Young, V. I. Utkin, and U. Ozguner, "A control engineer's guide to sliding mode control," *IEEE Trans. Control Syst. Technol.*, vol. 7, no. 3, pp. 28–342, May 1999.
- 34 J. Han, "From PID to active disturbance rejection control," *IEEE Trans. Ind. Electron.*, vol. 56, no. 3, pp. 900–906, Mar. 2009.
- 35 D. Won, W. Kim, and M. Tomizuka, "High-Gain-Observer-Based Integral Sliding Mode Control for Position Tracking of Electrohydraulic Servo Systems," *IEEE/ASME Trans. Mechatronics*, vol. 22, no. 6, pp. 2695–2704, Dec. 2017.
- 36 M. Ghanea, J. D. Leon, and A. Glumineau, "Cascade and high-gain observers comparison for sensorless closed-loop induction motor control," *IET Control Theory Appl.*, vol. 2, no. 2, pp. 133–150, Feb. 2008.
- 37 H. J. Sussmann, and P. V. Kokotovic, "The peaking phenomenon and the global stabilization of nonlinear systems," *IEEE Trans. Autom. Control*, vol. 36, no. 4, pp. 424–440, Apr. 1991.
- 38 J. Liu, S. Vazquez, L. Wu, A. Marquez, H. Gao, and L. G. Franquelo, "Extended State Observer-Based Sliding-Mode Control for Three-Phase Power Converters," *IEEE Trans. Ind. Electron.*, vol. 64, no. 1, pp. 22–31, Jan. 2017.
- 39 J. Liu, Y. Gao, X. Su, M. Wack, and L. Wu, "Disturbance-Observer-Based Control for Air Management of PEM Fuel Cell Systems via Sliding Mode Technique," *IEEE Trans. Control Syst. Technol.*, to be published, DOI 10.1109/TCST.2018.2802467.
- 40 J. C. Alexander, and J. H. Maddocks, "On the Kinematics of Wheeled Mobile Robots," *Int. J. Robot. Res.*, vol. 8, no. 5, pp. 15–27, Oct. 1989.
- 41 D. Ginoya, P. D. Shendge, and S. B. Phadke, "Sliding Mode Control for Mismatched Uncertain Systems Using an Extended Disturbance Observer," *IEEE Trans. Ind. Electron.*, vol. 61, no. 4, pp. 1983–1992, Apr. 2014.
- 42 T. D. Viet, P. T. Doan, N. Hung, H. K. Kim, and S. B. Kim, "Tracking control of a three-wheeled omnidirectional mobile manipulator system with disturbance and friction," *J. Mech. Sci. Technol.*, vol. 26, no. 7, pp. 2197–2211, Jul. 2012.
- 43 J. Yao, Z. Jiao, and D. Ma, "Extended-state-observer-based output feedback nonlinear robust control of hydraulic systems with backstepping," *IEEE Trans. Ind. Electron.*, vol. 61, no. 11, pp. 6285–6293, Nov. 2014.
- 44 H. K. Khalil, *Nonlinear Systems*, 3rd ed. Upper Saddle River, NJ: Prentice-Hall, 2002.
- 45 Z. Hou, L. Cheng, and M. Tan, "Decentralized Robust Adaptive Control for the Multiagent System Consensus Problem Using Neural Networks," *IEEE Trans. Syst., Man, Cybern. B, Cybern.*, vol. 39, no. 3, pp. 636–647, Jun. 2009.
- 46 J. Lee, S. Khoo, and Z. Wang, "DSP-Based Sliding-Mode Control for Electromagnetic-Levitation Precise-Position System," *IEEE Trans. Ind. Informat.*, vol. 9, no. 2, pp. 817–827, May 2013.
- 47 F. Esfandiari, and H. K. Khalil, "Output feedback stabilization of fully linearizable systems," *Int. J. Control.*, vol. 56, no. 5, pp. 1007–1037, 1992.
- 48 Y. Li, B. Yang, T. Zheng, Y. Li, M. Cui, and S. Peeta, "Extended-State-Observer-Based Double-Loop Integral Sliding-Mode Control of Electronic Throttle Valve," *IEEE Trans. Intell. Transp. Syst.*, vol. 16, no. 5, pp. 2501–2510, Oct. 2015.
- 49 K. Han, H. Kim, and J. S. Lee, "The sources of position errors of omni-directional mobile robot with Mecanum wheel," *IEEE Int. Conf. Syst., Man, Cybern.*, pp. 581–586, Oct. 2010.
- 50 M. Souzanchi-K, A. Arab, M. R. Akbarzadeh-T., and M. M. Fateh, "Robust impedance control of uncertain mobile manipulators using time-delay compensation," *IEEE Trans. Control Syst. Technol.*, vol. 26, no. 6, pp. 1942–1953, Nov. 2018.

9 Appendix

Considering a DC motor [50], it satisfies

$$L_a \dot{I}_a + R_a I_a + K_b \dot{\theta} = U, \quad (42)$$

where U and I_a are vector of motor voltages and vector of motor currents, respectively. Then the vector of motor torques τ is produced by the currents

$$\tau = K_m I_a, \quad (43)$$

Define $\nu = [Z_1^T \ Z_2^T \ I_a^T]^T$, $f(\nu_1, \nu_2) = (D_\theta J^+(\phi)M^{-1}J(\phi) + J^+(\phi)\dot{J}(\phi))[\dot{x}_q \ \dot{y}_q \ \dot{\phi}]^T + RJ^+(\phi)M^{-1}F$. In views of (12), (43) and (44), then one can obtain that

$$\dot{\nu} = A_\nu \nu + B_\nu U + C_\nu, \quad (44)$$

where

$$A_\nu = \begin{bmatrix} 0_{3 \times 3} & I_{3 \times 3} & 0_{3 \times 4} \\ 0_{3 \times 3} & 0_{3 \times 3} & K_m R J^+(\phi) M^{-1} \\ 0_{4 \times 4} & 0_{4 \times 4} & -\frac{R_a}{L_a} I_{4 \times 4} \end{bmatrix} \in \mathbb{R}^{10 \times 10},$$

$$B_\nu = \begin{bmatrix} 0_{3 \times 4} \\ 0_{3 \times 4} \\ \frac{1}{L_a} I_{4 \times 4} \end{bmatrix} \in \mathbb{R}^{10 \times 4}, \quad C_\nu = \begin{bmatrix} 0_{3 \times 1} \\ -f(\nu_1, \nu_2) + H \\ -\frac{K_b}{L_a} \dot{\theta} \end{bmatrix} \in \mathbb{R}^{10 \times 1}.$$